Size evolution of micropyrite from diagenesis to low-grade metamorphism

VÍCTOR CÁRDENES[1,4]*, RAÚL MERINERO[2], AURORA LÓPEZ-MUNGIRA[3], ÁLVARO RUBIO-ORDOÑEZ[4], IAIN K. PITCAIRN[5] & VEERLE CNUDDE[1]

[1]*Pore-scale Processes in Geomaterials Research Team (PProGRess), Ghent University, Krijgslaan 281 (S8), 9000 Ghent, Belgium*

[2]*Crystallography and Mineralogy Department, Complutense University of Madrid, Avda. Complutense s/n, 28040, Madrid, Spain*

[3]*Crystallography and Mineralogy Department, Extremadura University, Avda. de Elvas s/n, 06071 Badajoz, Spain*

[4]*Geology Department, Oviedo University, C/ Jesús Arias de Velasco s/n, 33005 Oviedo, Asturias, Spain*

[5]*Department of Geological Sciences, Stockholm University, SE-10691 Stockholm, Sweden*

V.C., 0000-0001-5246-7284

**Correspondence: cardenes@geol.uniovi.es*

Abstract: Size distribution and evolution of framboidal and euhedral microscopic crystals of pyrite (micropyrites, MPy) have been used for the last thirty years to deduce palaeo-redox conditions. The analysis of the MPy distributions can give valuable information about these palaeo-redox conditions. However, other information can also be retrieved from this type of analysis. In this work, we propose that the formation of new populations of MPy is a proxy of the transition from the anchizone to the epizone. High-resolution X-ray tomography (micro-CT) was used to determine the size distributions of MPy hosted in pelitic rocks subjected to different grades of low temperature metamorphism. These data were filtered and statistically analysed, which allowed us to find a statistical representative size distribution of the MPy present in the samples. The metamorphic grade was determined using the Kübler Index in combination with petrological and scanning electron microscopy (SEM) examination. The results show a relationship between metamorphic grade and MPy size distributions, and that new populations of MPy formed due to the effects of metamorphism. This new methodology for MPy size distribution has different potential applications in some fields of Earth sciences, such as palaeoenvironment reconstruction, ore mining or metamorphic petrology.

Pyrite is an iron sulphide mineral formed in a wide range of geological environments. One common texture of pyrite in the geological record is framboids: spherical clusters of nanocrystals with an average diameter of 5–20 μm but occasionally reaching sizes up to 250 μm (Sawlowicz 1993; Ohfuji *et al.* 2005; Merinero *et al.* 2009). Framboids can be used as markers for palaeo-redox conditions (Wilkin & Barnes 1996) but also as a sink for elements of economic interest (Large *et al.* 2012) and even as biomarkers (Wacey *et al.* 2014). Euhedral crystals of pyrite commonly occur with framboids (Wilkin *et al.* 1996). These may be the result of syn-metamorphic recrystallization of framboids (England & Ostwald 1993; Craig *et al.* 1998) or of hydrothermal activity (Graham & Ohmoto 1994). In this work, we use the term micropyrite (MPy) to describe both framboids and euhedral crystals. MPy sizes usually range from 2 to 50 μm diameter, reaching occasionally up to 350 μm.

The palaeo-redox environmental conditions can be inferred using different techniques, such as Fe–C–S relationships, sulphur isotope and metal traces data, fossil assemblage analysis, and size distribution and abundance of MPy populations. MPy size distributions were first measured by Wilkin *et al.* (1996) who used them to infer palaeo-redox conditions. In sedimentary environments, MPy can be formed from the first depositional stages, in the water column, until diagenesis, in the host sediments. Once

From: Ferrero, S., Lanari, P., Goncalves, P. & Grosch, E.G. (eds) *Metamorphic Geology: Microscale to Mountain Belts*. Geological Society, London, Special Publications, **478**,
https://doi.org/10.1144/SP478.2

these MPy have achieved diameters larger than 5–6 μm, they sink and are buried by the sediment (Wilkin & Barnes 1997; Bond & Wignall 2010). Depending on the palaeoenvironmental conditions, MPy may or may not continue to form on the sediment, producing different size distributions. Under euxinic conditions, MPy tends to be mainly framboids, with small size means (3–5 μm) and a narrow size distribution. Framboids formed under dysoxic conditions are larger (mean diameter >10 μm) and much more variable in size (Bond & Wignall 2010).

The size distribution of the sedimentary MPy populations, is thus a proxy of these palaeo-redox conditions (e.g. Wilkin & Barnes 1996; Suits & Wilkin 1998). Normally, this size distribution has been measured using microscopy techniques (i.e. scanning electron microscopy (SEM) and thin section examination). During metamorphism new populations of MPy may develop. These new populations form from available Fe and S, and rarely overgrow the pre-existing framboidal pyrite (e.g. Vokes 1969; Tempelman-Kluit 1970; Craig 1983; McClay & Ellis 1983; Sassano & Schrijver 1989; Craig & Vokes 1993; Craig *et al.* 1998; Large *et al.* 2007; Scott *et al.* 2009). In Fe-poor shales, deposited in euxinic to anoxic conditions, much or all of the available Fe may be converted to pyrite during early diagenesis. In such cases, any growth of pyrite during (closed-system) metamorphism would require dissolution of pre-existing MPy.

The metamorphic framboids do not morphologically differ from the sedimentary framboids, but sometimes it is possible to recognize overgrowth textures. Evolution from framboids to euhedral crystals together with increasing metamorphism has been demonstrated (England & Ostwald 1993; Sawlowicz 1993; Craig *et al.* 1998). This so-called evolution corresponds to morphological changes due to several processes, such as disappearance (via dissolution), recrystallization/replacement of original framboids, or the nucleation of pyrite overgrowths on the framboids. The increase in size modifies the original sedimentary MPy populations, which potentially lead to errors in the interpretation of the palaeo-redox conditions (Wacey *et al.* 2015). Scott *et al.* (2009) point out the difficulty of distinguishing the origin of framboids based on size distribution and shape. Some previous research, however, reports no clear relationship between prograde metamorphism and size increase in MPy populations. Using SEM and thin section examination, Ferry (1981) found no change in size of MPy as a function of the metamorphic grade, although this result may be a function of the uncertainty of the microscopy techniques used to measure the MPy populations, or perhaps the low availability of free Fe in the graphitic rocks studied. Scott *et al.* (2009), working with unmetamorphosed dolomitic shales, interpreted the largest framboids (>50 μm) to be of early diagenetic origin, while smallest framboids (<10 μm) would be of syn-metamorphic origin. However, the size distributions were not characterized and analysed in their work.

Hydrothermal processes can also form MPy. According to the laboratory experiments of Graham & Ohmoto (1994), the morphology is mainly cube-octahedrae, although framboids can be recognized. Hydrothermal processes can create new MPy using the earlier MPy (Large *et al.* 2009, 2012). England & Ostwald (1993) describe a morphological evolution from sedimentary to hydrothermal MPy framboids – atoll shapes – euhedrae. It is generally accepted that hydrothermal processes can create new populations of MPy with larger sizes and more euhedrae components. However, there are processes involved (formation temperature and mechanisms of pyrite deposition) that might lead to create a finer metamorphic MPy than the diagenetic MPy (Cline 2001). Some studies report that new framboids are indistinguishable from the sedimentary ones. Sassano & Schrijver (1989), working on carbonate rocks, reported framboid formation due to ferrous iron supplied by hydrothermal fluids and transported in the pore system. In the carbonate rocks used in this study, two genetic pulses of MPy (mainly framboids) were distinguished, early and late diagenetic. There was no distinction in size between both genetic pulses. Thirty size measures were performed, finding a size range from 2 to 30 μm (mean 15 μm). However, this work is focused on the genetic processes of the MPy, not on size evolution.

Another metamorphic reaction involving MPy is the gradual transformation from pyrite to pyrrhotite due to a process of desulphidation (Ferry 1981; Craig & Vokes 1993). Carpenter (1974) proposed the metamorphic isograd of pyrrhotite, which is close to the biotite isograd. The ratio pyrite/pyrrhotite decreases with the progression of metamorphism (Tempelman-Kluit 1970; Pitcairn *et al.* 2010), but this proportion is frequently modified by retrograde metamorphism, which induces the sulphidation of pyrrhotite, again forming pyrite. Regarding the effect of geological age on MPy size, Wilkin *et al.* (1997) measured MPy in Holocene sediments from the Black Sea, finding that 95% were less than 25 μm size and the 5% remaining up to 50 μm. Bond & Wignall (2010) found similar size intervals in sediments from the Permian–Triassic boundary. It is clear that the genetic processes that lead to sedimentary MPy formation are the same along the geological eras, even when the environmental conditions in some periods are more favourable. However, further geological processes (metamorphism and hydrothermalism) can have an effect on MPy size.

In summary, even though most of the authors agree that there is a relationship between increasing the size of MPy from diagenesis to metamorphism,

this relationship is not always clearly observed. One possible origin of this discrepancy could be the inaccuracy of microscopy techniques used for this purpose. These techniques generate data in 2D, which are not accurate enough to perform a methodical statistical analysis of size distribution of MPy. Recently, high-resolution X-ray tomography (micro-CT) has been successfully applied to the population analysis of MPy in low-grade pelitic rocks (Cárdenes *et al.* 2016). Together with a proper statistical analysis, micro-CT allows for measuring the size and number of all the MPy in a sample. This technique has been widely used in the field of Earth sciences (Cnudde & Boone 2013), especially in petrophysics, to characterize stone materials.

In this work, the populations of MPy were measured using micro-CT in several samples of pelitic rocks with different metamorphic grades, from diagenesis to medium-grade metamorphism (biotite isograd). The results were correlated with the Kübler Index (KI), or illite 'crystallinity', which is the standard method to determine the grade of metamorphism at low pressure–temperature (PT) conditions (Arkai *et al.* 2007). The micro-CT and KI data were complemented with SEM and optical microscopy examination of the samples.

Samples and methodology

Samples

Samples used in this work were roofing slates. A roofing slate is any rock used in construction, that can be split into large, thin and regular shingles due to the development of a penetrative cleavage (Cárdenes *et al.* 2014). On the other hand, a slate is an 'ultrafine or very fine-grained metamorphic rock displaying slaty cleavage' (Fettes *et al.* 2011, p. 40). Most roofing slates are slates *s.s.* indeed, but other rocks can be found, ranging from anchimetamorphism to medium-grade metamorphism: low-grade slates (argillites), slates, phyllites and mica-schists. Precursor mudstones are typically deposited under anoxic conditions. In fresh rock, the corresponding slates are black-grey, due to the occurrence of small amounts of organic matter (Cárdenes *et al.* 2012). Mudstones deposited under dysoxic to oxic conditions typically produce green to red slates, respectively (Potter *et al.* 2005).

For this work, sampling commercial types of roofing slates was considered advantageous as samples were unweathered and fresh, coming from easily accessible quarries with detailed geological studies, and free of hydrothermal influence, since hydrothermal processes usually inhibit the viability of a roofing slate quarry. Dykes, kink-bands and other structures affecting the massif homogeneity usually make it impossible to obtain slate shingles. Samples were therefore selected from among different commercial types of roofing slates (Table 1), according to their metamorphic grade (from low to medium grade), and with the same general palaeo-redox conditions, marked by grey-black colours.

Methodology

MPy populations were characterized using micro-CT. Basically, micro-CT is an imaging and analysis technique that differentiates the components of an object depending on their different attenuation to X-rays (Cnudde & Boone 2013). The large difference between the attenuation coefficient for pyrite and those of major minerals comprising the slate samples (e.g. quartz, mica and chlorite) allows

Table 1. *Description of samples*

Sample	Area	Stratigraphy	Period	Mineralogy*
BRA01	Minas Gerais, Brazil	Bambui Group	Ediacaran	Q, Ill, Chl (Py, Ca)
BRA02	Minas Gerais, Brazil	Bambui Group	Ediacaran	Q, Ill, Chl (Py, Ca)
GLE	Temiscouata, Canada	Bonavista Fm.	Cambrian	Ms, Q, Chl (Py, Ca)
RAT	Mayen, Germany	Dachschiefer Fm.	Devonian	Q, Ms, Chl (Py)
BRN	Bernardos, Spain	Santa Maria Beds	Cambrian	Q, Ms, Bt, Chl (Py, Ca)
LMO	Casaio, Spain	Pizarras de Luarca Fm.	Ordovician	Q, Ms, Chl (Py)
RIV	San Luis, Argentina	San Luis Fm.	Cambrian	Q, Bt, Ms, Chl (Py, Grt)

*Minerals are separated into main and accessory (in brackets). Abbreviations: Q, quartz; Ill, Illite; Chl, Chlorites; Ms, Muscovite; Bt, Biotite; Py, Pyrite; Ca, Calcite.

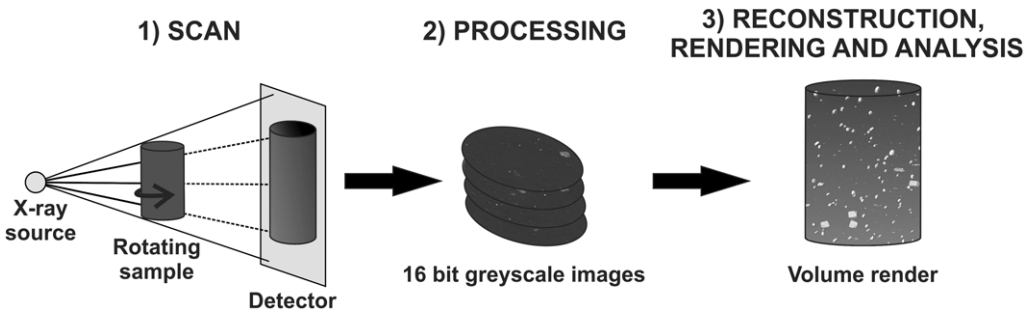

Fig. 1. Classic micro-CT setup (Cárdenes *et al.* 2016).

MPy to be readily differentiated in micro-CT imaging. The experimental setup consists of a sample rotating along the vertical axis while several X-ray projections (around 1800) are taken (Fig. 1). For the micro-CT scans, cylinders of 4 mm in diameter and 10 mm in length, with an approximate volume of 125 mm^3, were obtained from each sample using a diamond core drill. The cylinders were drilled so as to avoid sandy laminations or other heterogeneities present in some of the roofing slates. Samples were scanned at the Centre for X-ray Tomography of Ghent University (UGCT), Belgium, using the HECTOR setup (Masschaele *et al.* 2013) with a voltage of 130 kV and a tube power of 10 W, which achieves a resolution of 3 μm voxel. This resolution does not allow rendering of the crystallites composing the framboids, so the distinction between euhedrae and framboids is not straightforward. Data obtained were focused on the characterization of the size distribution of MPy. Obtained images were reconstructed and analysed with the programs Octopus Reconstruction v.8.8.2 and Octopus Analysis v.1.1.1.6. Size was estimated using the equivalent diameter criterion. The scanned average volume (125 mm^3) was considered to satisfy the representativeness of the measures, or representative elementary volume (REV), based on the results obtained for similar materials in Cárdenes *et al.* (2016).

The resulting population datasheets were analysed with the statistical software R v.3.1.2 and the mclust v.4.4 package (Fraley *et al.* 2012), which estimates the mixture and overlapping of the found populations. Lower intervals were adjusted to a lognormal distribution to avoid the micro-CT noise effect, which would add objects to the lower size intervals. This statistical approximation is based on the crystal size distribution theory (Eberl *et al.* 1998), which determines that the growth and size distributions of crystals can be adjusted to a lognormal distribution. According to this, the lowest intervals were adjusted to the inferred lognormal distribution. The abundance (number of objects per mm^3) was calculated after the interval adjustment. A more detailed explanation of this procedure can be found in Cárdenes *et al.* (2016).

Samples were also examined using a Zeiss Axio Scope A1 transmitted light microscope in order to determine their mineralogy and estimate mineral proportions. However, the volume of larger grains can be underestimated by this technique. Observations of the shape and arrangement of MPy were performed with a Hitachi TM 3000 SEM at the facilities of the company GEA Asesoría Geológica in Spain. Finally, the determination of the KI was performed at the facilities of the Analytical Services of the Extremadura University, Spain, following the recommendations of the IGPC 294 IC Working Group (Kisch 1991). The KI has been used by petrologists for many years, but has some disadvantages. The equipment must be calibrated with a standardized sample, following a special preparation procedure (Warr & Maehlmann 2015).

Results and discussion

The KI determination (Table 2) separated the samples into two groups: those (BRA01 and BRA02) belonging to the anchizone in the boundary between metamorphism and diagenesis (0.42–0.25 KI), and those (GLE, RAT, BRN, LMO and RIV) belonging to the epizone (<0.25 KI) in the field of greenschist facies metamorphism (or above, i.e. 300°C). This differentiation was confirmed by the petrological analysis (Table 1). The anchizone samples have a moderately developed cleavage parallel to bedding, which is sufficient to facilitate splitting into shingles. However, the KI results showed that they are indeed metamorphic rocks, i.e. subjected to temperatures equivalent to prehnite–pumpellyite facies of region metamorphism. The epizone samples have a well-developed, penetrative cleavage of undoubted metamorphic character. Petrographical examination showed the same assemblage of main minerals (Table 1) for all the samples (quartz, chlorite and mica). Higher metamorphic grades are suggested

Table 2. *Results of the statistical analysis of micro-CT data (units in μm), and KI*

Sample	Micro-CT							Kübler Index	
	Pop.*	Mean	% Vol.†	SD	*N*	Abundance	Max‡	Value	Zone
BRA01	P0	16.8	100	7.8	1755	22.5	66	0.32	Anchizone
BRA02	P0	15.3	100	5.8	5389	52.5	63	0.41	Anchizone
GLE	P0	16.8	100	7.8	8868	105.4	66	0.19	Epizone
RAT	P0	9.9	83.2	3.3	12 149	151.6	18	0.19	Epizone
	P1	19	16.8	12.9	2453	30.6	288		
BRN	P0	14.9	60.5	5.0	2086	29.7	36	0.19	Epizone
	P1	25.8	39.5	13.7	1362	19.4	132		
LMO	P0	16.7	51.1	5.7	689	5.0	33	0.12	Epizone
	P1	43.3	48.9	27.3	660	4.8	237		
RIV	P0	12.1	91.3	4.6	11 149	150.6	18	0.05	Epizone
	P1	15	8.7	12.9	1066	14.4	336		

*Different subpopulations found by the statistical analysis.
†Percentage of volume for each subpopulation.
‡Maximum size of the measured population.

by the presence of biotite in BRN and RIV. Garnet also occurs in RIV, which returned the lowest KI value of any of the samples (Table 2). The mineral assemblage in sample RIV suggests peak temperatures of 450–500°C.

The MPy could be distinguished with the optical microscope at ×500 magnification (Fig. 2a). MPy were found in two different arrangements: uniformly scattered all over the sample, and grouped in clusters, frequently surrounded by quartz along the sedimentation planes. The occurrence of these MPy clusters might hinder the interpretation of the size increase of single MPy. For this reason, the samples were chosen in areas without these clusters. SEM examination also showed the presence of MPy without overgrowths and dissolution features (Fig. 2b) in all samples.

The statistical analysis of the size populations obtained by micro-CT showed a clear tendency for maximum size increase along with the metamorphism, as well as the development of a second population at the epizone (Table 2). This analysis discriminated a single population of MPy (P0), in anchizone and sample GLE, and two populations of MPy (P0 and P1) in the rest of the samples (Fig. 3). The lognormal Q–Q plots (Fig. 4) show a good correlation between observed size distributions and the theoretical lognormal distribution for the samples with lowest metamorphism (BRA01, BRA02 and GLE). For samples with higher metamorphism (RAT, BRN, LMO and RIV) there is a right skew in the lognormal Q–Q plots, towards larger sizes. This skew shows the occurrence of a second population P1. It is not possible to distinguish

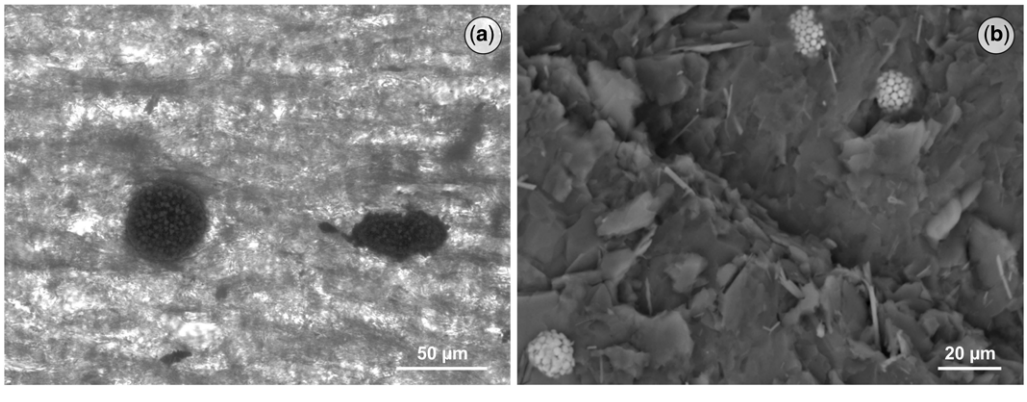

Fig. 2. (**a**) Two pyrite framboids from sample LMO. Optical microscopy of transmitted light, ×500. (**b**) SEM image of several pyrite framboids in sample RAT.

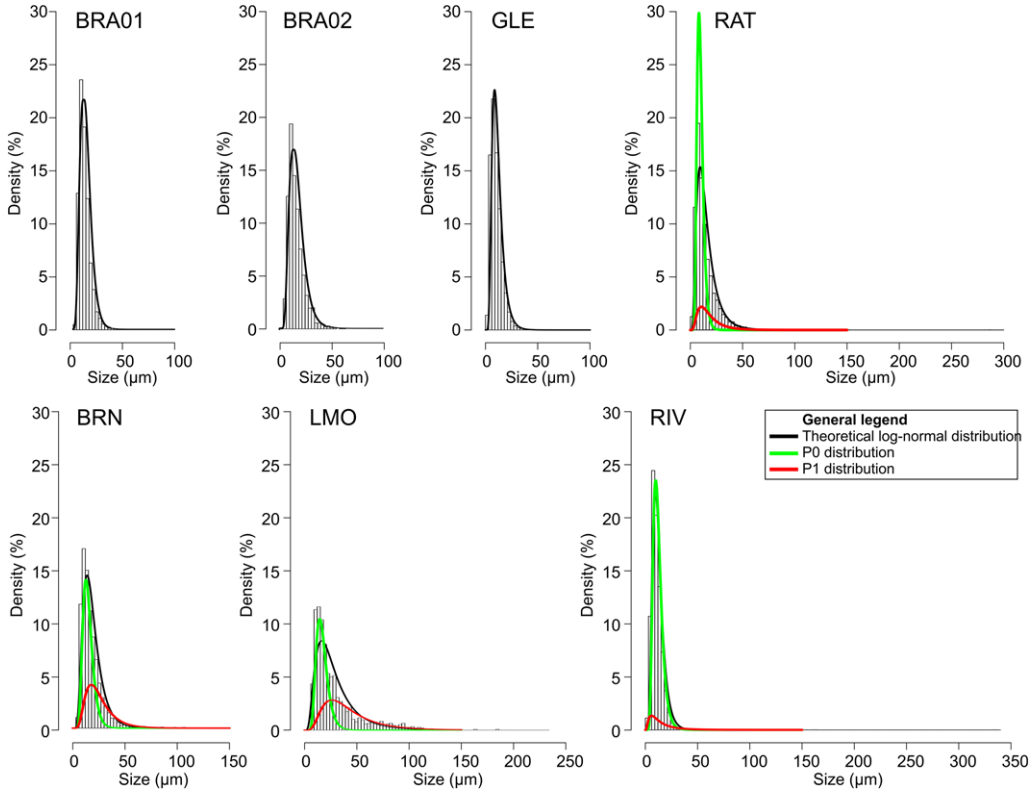

Fig. 3. Size histograms of the MPy determined by micro-CT. For BRA01, BRA02 and GLE, only one population was detected. These three samples belong to the anchizone (BRA01 and BRA02) and to the epizone (GLE). For the rest of the samples, two populations, P0 and P1were detected. P0 (green line) is attributed to sedimentary MPy, while P1 (red line) is attributed to metamorphic MPy. The theoretical lognormal distribution is marked by the black line.

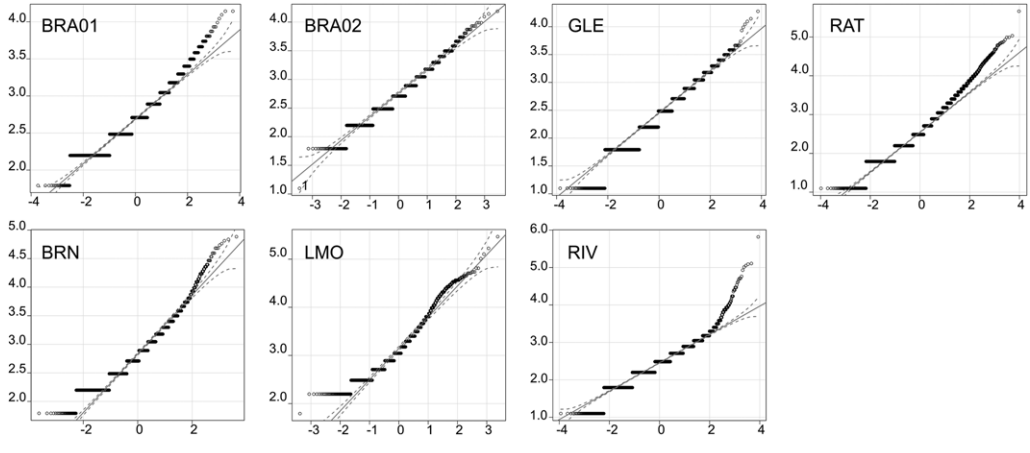

Fig. 4. Lognormal Q–Q plots showing the adequacy of the inferred size distributions (dots) to the theoretical lognormal distribution (line).

between sedimentary and metamorphic populations from the distribution of sizes of MPy.

The abundance of objects does not show a clear variation with metamorphism. At the anchizone, abundance of MPy ranges from 22.5 to 52.5 objects per mm^3, while for the epizone abundances range from 4.8 to 151.6. This poor correlation is probably due to compositional differences between the protoliths, which are certainly from different sources. Finally, no correlation was found between the age of the slate and the size of the MPy.

Conclusions

The measurement and analysis of micropyrites (MPy) in several roofing slates with different grades of metamorphism has highlighted the development of a second MPy population. The development of secondary MPy populations can also be used as a proxy to define the transition from the anchizone, typically with only one population of MPy, to the epizone with two populations. This work describes how MPy population analysis can be conducted by means of high-resolution X-ray tomography together with statistical analysis. This methodology provides data about the size distribution of the existing populations of MPy in a fast and accurate way, and to differentiate between overlapped populations of MPy objects that might complicate the interpretation of the palaeo-redox conditions. On the other hand, the equipment required (X-ray micro tomography setup) is not easily available. When working on metamorphic rocks, the data provided by micro-CT should be complemented with other methods, like the determination of the KI, and SEM and petrographic analysis.

Acknowledgements Thanks to Dr Robert Scott for his valuable comments that greatly improved this manuscript.

Funding Victor Cárdenes is grateful for the IEF Marie Curie Grant 623082 TOMOSLATE from the European Research Council.

References

Arkai, P., Sassi, F.P. & Desmons, J. 2007. Very low- to low-grade metamorphic rocks. *In*: Fettes, D. & Desmons, J. (eds) *Metamorphic Rocks. A Classification and Glossary Terms*. Cambridge University Press, Cambridge, 36–42.

Bond, D.P.G. & Wignall, P.B. 2010. Pyrite framboid study of marine Permian-Triassic boundary sections: a complex anoxic event and its relationship to contemporaneous mass extinction. *Geological Society of America Bulletin*, **122**, 1265–1279, https://doi.org/10.1130/b30042.1

Cárdenes, V., Prieto, B., Sanmartín, P., Ferrer, P., Rubio, A. & Monterroso, C. 2012. The influence of chemical-mineralogical composition on the color and brightness of Iberian roofing slates. *Journal of Materials in Civil Engineering*, **24**, 460–467, https://doi.org/10.1061/(ASCE)MT.1943-5533.0000396

Cárdenes, V., Rubio-Ordoñez, A., Wichert, J., Cnudde, J.P. & Cnudde, V. 2014. Petrography of roofing slates. *Earth-Sciences Reviews*, **138**, 435–453, https://doi.org/10.1016/j.earscirev.2014.07.003

Cárdenes, V., Merinero, R. *et al.* 2016. Characterization of micropyrite populations in low-grade metamorphic slate: a study using high-resolution X-ray tomography. *Palaeogeography, Palaeoclimatology, Palaeoecology*, **441**, 924–935, https://doi.org/10.1016/j.palaeo.2015.10.044

Carpenter, R.H. 1974. Pyrrhotite Isograd in Southeastern Tennessee and Southwestern North Carolina. *Geological Society of America Bulletin*, **85**, 451–456, https://doi.org/10.1130/0016-7606(1974)85<451:PIISTA>2.0.CO;2

Cline, J.S. 2001. Timing of gold and arsenic sulfide mineral deposition at the Getchell Carlin-type gold deposit, north-central Nevada. *Economic Geology and the Bulletin of the Society of Economic Geologists*, **96**, 75–89, https://doi.org/10.2113/gsecongeo.96.1.75

Cnudde, V. & Boone, M.N. 2013. High-resolution X-ray computed tomography in geosciences: a review of the current technology and applications. *Earth-Science Reviews*, **123**, 1–17, https://doi.org/10.1016/j.earscirev.2013.04.003

Craig, J.R. 1983. Metamorphic features in Appalachian massive sulfides. *Mineralogical Magazine*, **47**, 515–525, https://doi.org/10.1180/minmag.1983.047.345.13

Craig, J.R. & Vokes, F.M. 1993. The metamorphism of pyrite and pyritic ores – an overview. *Mineralogical Magazine*, **57**, 3–18, https://doi.org/10.1180/minmag.1993.057.386.02

Craig, J.R., Vokes, F.M. & Solberg, T.N. 1998. Pyrite: physical and chemical textures. *Mineralium Deposita*, **34**, 82–101, https://doi.org/10.1007/s001260050187

Eberl, D.D., Drits, V.A. & Srodon, J. 1998. Deducing growth mechanisms for minerals from the shapes of crystal size distributions. *American Journal of Science*, **298**, 499–533.

England, B.M. & Ostwald, J. 1993. Framboid-derived structures in some Tasman fold belt base-metal sulfide deposits, New-South-Wales, Australia. *Ore Geology Reviews*, **7**, 381–412, https://doi.org/10.1016/0169-1368(93)90002-g

Ferry, J.M. 1981. Petrology of graphitic sulfide-rich-schists from south-central Maine – an example of de-sulfidation during prograde regional metamorphism. *American Mineralogist*, **66**, 908–931.

Fettes, D.J., Desmons, J. & Árkai, P. 2011. *Metamorphic Rocks: A Classification and Glossary of Terms. Recommendations of the International Union of Geological Sciences Subcommission on the Systematics of Metamorphic Rocks*. Cambridge University Press, Cambridge.

Fraley, C., Raftery, A.E., Murphy, T.B. & Scrucca, L. 2012. *mclust Version 4 for R: Normal Mixture*

Modeling for Model-Based Clustering, Classification, and Density Estimation. Department of Statistics, University of Washington.

Graham, U.M. & Ohmoto, H. 1994. Experimental study of formation mechanisms of hydrothermal pyrite. *Geochimica et Cosmochimica Acta*, **58**, 2187–2202, https://doi.org/10.1016/0016-7037(94)90004-3

Kisch, H.J. 1991. Illite crystallinity: recommendations on sample preparation, X-ray diffraction setting, and interlaboratory samples. *Journal of Metamorphic Geology*, **9**, 665–670.

Large, R., Thomas, H., Craw, D., Henne, A. & Henderson, S. 2012. Diagenetic pyrite as a source for metals in orogenic gold deposits, Otago Schist, New Zealand. *New Zealand Journal of Geology and Geophysics*, **55**, 137–149, https://doi.org/10.1080/00288306.2012.682282

Large, R.R., Danyushevsky, L. *et al.* 2009. Gold and trace element zonation in pyrite using a laser imaging technique: implications for the timing of gold in orogenic and Carlin-style sediment-hosted deposits. *Economic Geology*, **104**, 635–668.

Large, R.R., Maslennikon, V.V., Robert, F., Danyushevsky, L.V. & Chang, Z. 2007. Multistage sedimentary and metamorphic origin of pyrite and gold in the giant Sukhoi Log deposit, Lena gold province, Russia. *Economic Geology*, **102**, 1233–1267, https://doi.org/10.2113/gsecongeo.102.7.1233

Masschaele, B., Dierick, M. *et al.* 2013. HECTOR: a 240 kV micro-CT setup optimized for research. *Journal of Physics Conference Series*, **463**, 012012, https://doi.org/10.1088/1742-6596/463/1/012012

McClay, K.R. & Ellis, P.G. 1983. Deformation and recrystallization of pyrite. *Mineralogical Magazine*, **47**, 527–538, https://doi.org/10.1180/minmag.1983.047.345.14

Merinero, R., Lunar, R., Somoza, L., Diaz-Del-Rio, V. & Martinez-Frias, J. 2009. Nucleation, growth and oxidation of framboidal pyrite associated with hydrocarbon-derived submarine chimneys: lessons learned from the Gulf of Cadiz. *European Journal of Mineralogy*, **21**, 947–961, https://doi.org/10.1127/0935-1221/2009/0021-1956

Ohfuji, H., Boyle, A.P., Prior, D.J. & Rickard, D. 2005. Structure of framboidal pyrite: an electron backscatter diffraction study. *American Mineralogist*, **90**, 1693–1704, https://doi.org/10.2138/am.2005.1829

Pitcairn, I.K., Olivo, G.R., Teagle, D.A.H. & Craw, D. 2010. Sulfide evolution during prograde metamorphism of the Otago and Alpine schists, New Zealand. *Canadian Mineralogist*, **48**, 1267–1295, https://doi.org/10.3749/canmin.48.5.1267

Potter, P.E., Maynard, J.B. & Depetris, P.J. 2005. *Mud & Mudstones. Introduction and Overview*. Springer, Berlin, 55–74.

Sassano, G.P. & Schrijver, K. 1989. Framboidal pyrite: Early-diagenetic, Late-diagenetic, and hydrothermal occurrences from the acton vale quarry, Cambro-Ordovician, Quebec. *American Journal of Science*, **289**, 167–179.

Sawlowicz, Z. 1993. Pyrite framboids and their development: a new conceptual mechanism. *International Journal of Earth Sciences*, **82**, 148–156.

Scott, R.J., Meffre, S., Woodhead, J., Gilbert, S.E., Berry, R.F. & Emsbo, P. 2009. Development of framboidal pyrite during diagenesis, low-grade regional metamorphism, and hydrothermal alteration. *Economic Geology*, **104**, 1143–1168.

Suits, N.S. & Wilkin, R.T. 1998. Pyrite formation in the water column and sediments of a meromictic lake. *Geology*, **26**, 1099–1102, https://doi.org/10.1130/0091-7613(1998)026<1099:pfitwc>2.3.co;2

Tempelman-Kluit, D.J. 1970. Relationship between sulfide grain size and metamorphic grade of host rocks in some strata-bound pyritic ores. *Canadian Journal of Earth Sciences*, **7**, 1339–1345, https://doi.org/10.1139/e70-127

Vokes, F.M. 1969. A review of metamorphism of sulphide deposits. *Earth-Science Reviews*, **5**, 99–143, https://doi.org/10.1016/0012-8252(69)90080-4

Wacey, D., Saunders, M., Cliff, J., Kilburn, M.R., Kong, C., Barley, M.E. & Brasier, M.D. 2014. Geochemistry and nano-structure of a putative similar to 3240 million-year-old black smoker biota, Sulphur Springs Group, Western Australia. *Precambrian Research*, **249**, 1–12, https://doi.org/10.1016/j.precamres.2014.04.016

Wacey, D., Kilburn, M.R. *et al.* 2015. Uncovering framboidal pyrite biogenicity using nano-scale CNorg mapping. *Geology*, **43**, 27–30, https://doi.org/10.1130/g36048.1

Warr, L.N. & Maehlmann, R.F. 2015. Recommendations for Kubler Index standardization. *Clay Minerals*, **50**, 283–286, https://doi.org/10.1180/claymin.2015.050.3.02

Wilkin, R.T. & Barnes, H.L. 1996. Pyrite formation by reactions of iron monosulfides with dissolved inorganic and organic sulfur species. *Geochimica et Cosmochimica Acta*, **60**, 4167–4179, https://doi.org/10.1016/s0016-7037(97)81466-4

Wilkin, R.T. & Barnes, H.L. 1997. Formation processes of framboidal pyrite. *Geochimica et Cosmochimica Acta*, **61**, 323–339.

Wilkin, R.T., Barnes, H.L. & Brantley, S.L. 1996. The size distribution of framboidal pyrite in modern sediments: an indicator of redox conditions. *Geochimica et Cosmochimica Acta*, **60**, 3897–3912, https://doi.org/10.1016/0016-7037(96)00209-8

Wilkin, R.T., Arthur, M.A. & Dean, W.E. 1997. History of water-column anoxia in the Black Sea indicated by pyrite framboid size distributions. *Earth and Planetary Science Letters*, **148**, 517–525, https://doi.org/10.1016/S0012-821X(97)00053-8